UCRL-JC-131664
PREPRINT

The Role of Twinning in the Optimization of the Grain Boundary Character Distribution

Mukul Kumar
Adam J. Schwartz
Wayne E. King

This paper was prepared for submittal to the
International Symposium on Advances in Twinning
TMS-AIME Annual Meeting
San Diego, CA
February 28 - March 4, 1999

January 8, 1999

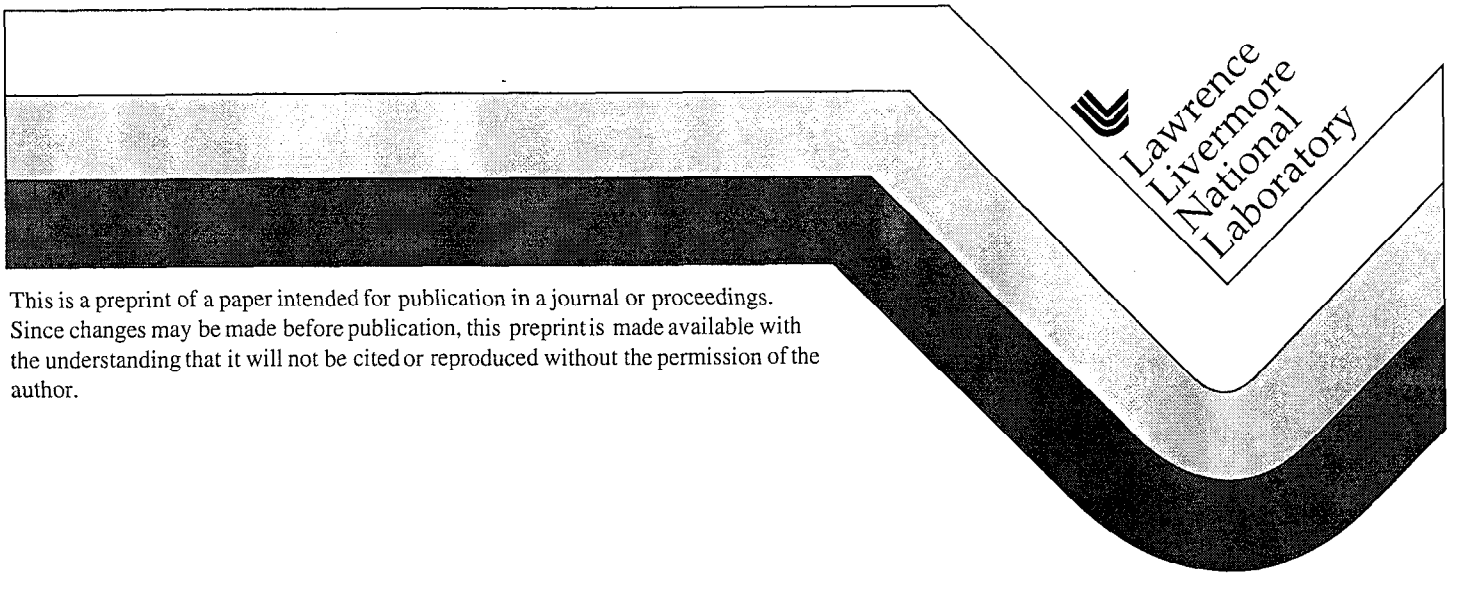

THE ROLE OF TWINNING IN THE OPTIMIZATION OF THE GRAIN BOUNDARY CHARACTER DISTRIBUTION

Mukul Kumar, Adam J. Schwartz, and Wayne E. King

Lawrence Livermore National Laboratory, University of California
7000 East Avenue, L-370, Livermore, CA 94550

ABSTRACT

The grain boundary character distribution (GBCD) is a microstructural property that describes the proportions of "special" and "random" boundaries as defined by the coincident site lattice model. Recently, there has been increased attention on determination of the GBCD and manipulation of the relative fractions in the microstructure through thermomechanical processing in order to improve material's properties like corrosion and creep resistance. Most of the "optimization" treatments reported in the literature have been performed on fcc materials with relatively low stacking fault energies and have resulted in microstructures with high fractions of $\Sigma 3$, $\Sigma 9$, and $\Sigma 27$ boundaries. It could be interpreted that annealing twins are solely required to improve the GBCD. However, in order to optimize the properties, it appears imperative that the formation of annealing twins disrupt the connectivity of the random boundary network, thus implying that $\Sigma 3^n$ reactions and resultant triple lines are critical. Experiments to modify the GBCD of oxygen–free electronic Cu and Inconel 600 through thermomechanical processing are presented and discussed in light of observations of the deformed and recrystallized microstructures.

INTRODUCTION

Many important physical and mechanical properties of materials are known to be intimately coupled to microstructural features such as chemistry, grain size and shape, texture, and the presence of secondary phases and precipitates. Intercrystalline defects, such as grain boundaries and triple lines or junctions, have been observed to exert a significant influence on corrosion resistance [1,2], stress corrosion cracking [3], creep [4,5], total elongation to failure [5], fracture [6] and the morphology and type of grain boundary precipitates [7]. Numerous reports in the literature, including a broad overview by several groups of authors [8], have demonstrated that it is possible to exert control over the types of grain boundaries in the microstructure of different materials. Thus, in principle, it allows tailoring of properties for specific applications in a manner similar to modifications of the microstructure through solid-state phase transformations.

Watanabe [9] was the first to use the term "grain boundary design and control", which has evolved to the concept of "grain boundary engineering". To date, efforts to engineer grain boundaries have primarily concentrated on changing the misorientation distribution function (MDF) through thermomechanical processing so as to increase the fraction of grain boundaries in the microstructure which exhibit orientations characterized by the coincident site lattice (CSL) model [10]. In the CSL model, the grain boundary is characterized by the misorientation of the grains on either side of it, and the plane of the grain boundary is neglected. There has been much discussion regarding the relative importance of grain boundary planes *vs.* grain misorientations in affecting properties, and the reader is referred to a recent overview by Randle [11] for further details. In particular, it relates to the differences that are engendered when considering orientation relationships between lattices motifs in neighboring grains as opposed to the inter-relationship between boundary surfaces themselves. Clearly, grain boundary planes with the highest density of coinciding sites are preferred (to minimize the free volume at the boundaries), and this criterion is met on consideration of low–Σ CSL (or special) boundaries, where Σ refers to the reciprocal density of coincident sites. This issue will not be discussed further and the CSL model for grain boundary character distribution will be utilized for its convenience, and also because it provides common ground with previous works.

Fundamentally, grain boundary engineering involves thermomechanical processing (TMP); deformation–induced strain and annealing. During annealing, the intent is to replace random boundaries with special boundaries in the boundary network. When the appropriate processing conditions are obtained, grain boundary engineering appears to produce materials where the grain size gets refined, the fraction of special boundaries increases, and the deviations from exact CSL misorientations decrease. Despite these changes to the microstructure, there is no significant increase in the observed texture; in fact, the texture strength may actually be reduced.

This randomization of texture components has been known for some time in the context of multiple twinning [12] in low or medium stacking fault energy fcc metals and alloys; typically, Cu- or Ni-based systems or austenitic stainless steels. It has been conclusively shown that the proportion of annealing twin ($\Sigma 3$) boundaries increases in the microstructure on recrystallization. This occurs as secondary twinning events leading to multiple twin formation in the same grain become increasingly more likely due to favorable grain re-orientation by primary twin formation. In fact, it is considered that annealing twinning is the only mechanism by which new orientations are generated during recrystallization of fcc materials, with the initial orientations being contained in the deformation microstructure prior to annealing [13]. It has also been shown [13] that twin boundaries can either be formed perpendicular or parallel to the recrystallization front, but the selection of one mechanism over the other has not been clarified. Not coincidentally perhaps, attempts at grain boundary engineering have been largely restricted to those alloy systems where there is a propensity for the formation of annealing twins during static recrystallization.

The observed improvements in properties, it would appear, result from an alteration to the grain boundary network such that the existence of a high fraction of special grain boundaries interrupts the connectivity of the random grain boundaries. However, a clear correlation between properties of the so-called "optimized" material and connectivity of grain boundaries has not been reported to date, though several studies [8] have drawn conclusions

based on the increased proportion of special boundaries in the microstructure. It is now recognized that, while the increase in the fraction of special boundaries is desirable, the benefits of such an increase can only be considered in the context of the network of triple junctions that these boundaries are a part of. Thus it has been postulated that the idealized planar microstructure can be entirely composed of a network of $\Sigma 3$ and $\Sigma 9$ boundaries, in the proportion 2:1, the so-called twin-limited microstructure [14,15]. The $\Sigma 9$ boundaries are geometrically necessary to maintain the integrity of the triple junctions formed by the intersection of two $\Sigma 3$ boundaries. It is further envisaged that the complete microstructure can be mapped by the formation of $\Sigma 3^n$ type of boundaries, where n is an integer that takes values from 0 to 3 [14-16]. The higher order $\Sigma 3$ derivatives are a direct consequence of twin-twin interactions, while the low-angle $\Sigma 1$ boundaries are equally probable from rotational geometry at the triple junctions. The twin boundary derivatives beyond $\Sigma 27$ are not considered to be as desirable due to considerably decreased coincidence of lattice sites beyond an arbitrary cut-off value of $\Sigma 29$ or $\Sigma 49$, as first suggested by Palumbo and Aust [17].

Advances in the engineering of grain boundaries in materials have been facilitated in recent years by the commercialization of a scanning electron microscope (SEM) technique for automatic indexing of Kikuchi backscattered electron diffraction patterns known as Orientation Imaging Microscopy (OIM) [18-20]. This technique has superseded other experimental techniques, such as transmission electron microscopy (TEM) and electron channeling patterns in SEM, for the determination of the GBCD due to the relatively straightforward specimen preparation and the large number of orientation measurements attainable in a relatively short period of time. Thus, advances in engineering of grain boundaries can be ascribed due to the following factors: (1) recognition that grain boundaries play an important role in a number of materials properties, (2) recent evidence that thermomechanical processing can alter the GBCD, and (3) ease of characterization of the GBCD by the OIM technique.

Two fundamentally different paths to grain boundary engineering have been reported thus far in the literature. One approach has been to strain the material to small to moderate levels on the order of 6-8%, followed by annealing at temperatures low enough to prevent recrystallization yet cause reorientation of grain boundaries towards lower energy configurations, *i.e.*, low Σ boundaries [14,21,22]. This approach while appearing to increase the fraction of special boundaries is commercially impractical in that it requires very lengthy annealing times on the order of 10-15 hours. Moreover, it leads to the undesirable side effect of increasing the grain size quite considerably owing to the long annealing treatments [23,24]. A further drawback appears to be the inability to adequately "seed" favorable orientations in the deformation microstructure at such low strain levels. It has been shown, however, that this "fine tuning" approach considerably reduces the deviation of the grain boundaries from the exact CSL crystallographic description, as set by the Brandon criterion [25].

The second approach attempts to side-step these drawbacks by resorting to a multi-cycle treatment of moderate strain levels with annealing treatments at relatively high temperatures but for very short times, which could be on the order of 5 to 15 minutes. An important aspect of this approach is the total forming reduction being broken up into several cycles of strain and recrystallization. Thus, only primary recrystallization is effected in the short annealing times and subsequent grain growth that would be initiated at the high temperatures is partially or completely avoided. Thus the fraction of special boundaries is increased in the final microstructure without an increase in the grain size of the material, though it is strictly not clear whether recrystallization and grain growth do or do not occur simultaneously during the annealing process. The efficacy of such an approach has been demonstrated in several studies with the proportion of special boundaries exceeding 80% in some cases. However, as mentioned earlier, these data have not been correlated with the spatial distribution of grain boundaries at triple points in the microstructure.

This paper describes the different approaches to the engineering of grain boundaries that are part of an on-going research program investigating low and medium stacking fault energy fcc materials as well as bcc materials. A brief description of the materials selection and processing and OIM data analysis is presented. The experimental results, some of which have been reported earlier [23,24], will be described in the light of theoretical postulates that have been proposed for distributions of grain boundary character and triple junctions. A critical assessment will be reported based on the connectivity of grain boundaries that is represented by the triple junction distribution.

MATERIALS SELECTION AND PROCESSING

The effects of TMP on the grain boundary character and triple junction distributions have been examined in oxygen free electronic (ofe) Cu and Inconel 600. Starting material specifications and processing sequences are described in this section. A Hitachi C10100 oxygen free electronic (99.99%) Cu bar, with the measured impurity concentration as listed in Table I, was used for both the strain-annealing and strain-recrystallization processes. Elemental analysis for the Inconel 600 alloy is also listed in Table I.

Table I. Elemental analysis for ofe-Cu and Inconel 600 materials.

Oxygen Free Electronic Copper		Inconel 600	
Element	Concentration (ppm)	Element	Concentration (wt%)
H	0.90	Ni	74.650
C	5.0	Cr	16.20
O	6.0	Mn	0.240
Si	0.20	Si	0.280
P	0.4	Ti	0.20
S	4.0	Cu	0.010
Fe	2.0	Fe	8.0
Ni	1.0	S	0.0020
As	0.40	P	0.0070
Se	0.30	Al	0.190
Ag	6.40	Co	0.050
Sb	0.30	B	0.0010
Pb	0.20	C	0.0640

The first thermomechanical processing series on Cu focussed on strain annealing (SA). Small deformations, less than 7%, were induced by uni-axial compression followed by long time anneals. The starting condition for this series of experiments was ofe-Cu that was forged 50%, annealed for 4 hours in vacuum at 375°C, forged 40%, rolled 200%, and annealed for one hour in vacuum at 375°C. Sample coupons approximately 10 X 10 X 9 mm^3 were cut from the plate and prepared for OIM observation using standard metallographic techniques. The samples were lapped and polished to remove a sufficient thickness of material to ensure that the subsequent OIM scan examined bulk material. The GBCD of the starting material was also determined using OIM.

Table II. Process sequence for strain annealing treatments.

	Sample/ Process Number				
Process	ReX-Cu	SA-1	SA-2	SA-3	SA-4
Strain		~7%	~6%	~6%	~6%
Heat	See text	334°C/8 h	275°C/14 h	225°C/14 h	325°C/6 h
Treatment		532°C/14 h	375°C/7 h	325°C/ 6 h	
Grain Size	10 μm	75 μm	65 μm	55 μm	30 μm

Following the strain-annealing work of Thompson and Randle [22], the specimens were deformed approximately 6% in compression in an attempt to localize deformation at specific locations in the microstructure. The lightly deformed samples were characterized by OIM, followed by a two-stage heat treatment, as shown in Table II, in an attempt to optimize the GBCD. The temperatures and times for the first strain-annealing treatment, SA-1 were scaled to the melting point of Cu from the work of Thompson and Randle on Ni [22]. The temperatures of SA-2 were obtained by scaling the temperature used by Thompson and Randle for Ni relative to the recrystallization temperature. The temperatures of SA-3 were selected to probe the effect of lower temperatures while aiming to minimize grain growth. A single temperature was chosen for SA-4 to probe the effects of the lower temperature anneal.

Repeated or sequential strain-recrystallization (SR) processing was the focus of the second series of experiments. Strain-recrystallization applies moderate levels of deformations (between 20 and 30%) followed by intermediate or high temperature anneals. In this series, the starting material was a Hitachi Cu bar, with a similar impurity content to that listed in Table I,

that was 38 mm in diameter and 76 mm long. This was in the semi-hard condition and was further deformed 30% in compression. Specimen disks, 10 mm thick, were extracted from the center of the bar, and sectioned into fourths. These specimens were then annealed in an argon sand bath at temperatures between 350 and 400°C for 10 minutes as described in Table III. After water quenching, the specimens were prepared for optical metallography and OIM taking care to remove sufficient material from the surface to ensure characterization of bulk grains in the interior of the specimen. After OIM characterization, each of the specimens was again compressed 30% and annealed. This process was repeated for three full strain-recrystallization treatments.

Table III. Process sequence for ofe-Cu strain-recrystallization treatments.

	Sample/Process Number		
Process	OFE-AR	SR-350	SR-400
Strain	As-received	~30%	~30%
Heat Treatment	None	350°C/10 min	400°C/10 min
Grain Size	125 μm	27 μm	35 μm

An Inconel 600 alloy, with a nominal composition as given in Table I, was chosen in order to examine an alloy with the fcc crystal structure but with a different stacking fault energy. The starting material was a bar 406 mm in length, with a square cross-section 25 X 25 mm^2. The bar was sectioned into four pieces approximately 100 mm long, leaving an additional section 7 mm long for optical metallography and OIM preparation. The purpose of the metallography was to characterize the grain structure after each processing step. Each section was then subjected to sequential thermomechanical processing, (deformation by rolling, then annealing). The series of optimization treatments induced a thickness reduction of 20% per rolling sequence. The bar was annealed at 1000°C for 15 minutes in air followed by water quenching. At this point, a section 13 mm in length was cut from one of the ends for metallography and OIM sample preparation. A similar sequence of straining followed by a high temperature-short time anneal was performed for a total of 7 times. OIM observations were made after step number 1, 3, 4, 5, and 7 for a total of six observations including the as-received condition.

DATA ACQUISITION AND ANALYSIS

Orientation Imaging Microscopy (OIM) is an SEM technique that automatically acquires and processes electron backscattered Kikuchi diffraction patterns (EBSP's) for determination of local orientations, misorientations, and microtexture. OIM allows the orientation at spatially specific points in the microstructure to be measured and directly correlated with results from other imaging techniques such as optical or scanning electron microscopy. The formation of an EBSP requires a highly collimated, stationary electron probe focused on a steeply inclined specimen. The interaction of the electron beam and the specimen generates an EBSP by the backscattering of electrons from favorably oriented crystal planes. The diffraction pattern is collected on a phosphor screen that is coupled via a fiber-optic bundle to a low-light-level silicon-intensified camera. The EBSP image is frame-averaged and the background intensity is subtracted by an image processor. The digitized diffraction pattern is indexed by the workstation.

In the OIM technique, individual orientation measurements are made at discrete points on a sample; the locations of the points are defined by a grid of dimensions prescribed by the user (both in the width and height of the grid as well as the spacing between points on the grid). At each point in the grid, the backscatter Kikuchi diffraction pattern is captured, frame averaged and automatically indexed. The three Euler angles that describe the orientation are recorded along with coordinates describing the position. Thus, images (or maps) can be generated by mapping the crystal orientation onto a color or gray scale and shading each point on the grid according to some aspect of the crystal orientation. Alternatively, misorientations between points can be indicated by drawing boundaries that are color coded by type of boundary, for example, special or random.

Samples were observed in a Hitachi S2700 SEM with an automated OIM attachment (TSL, Inc.) [26]. Typically, OIM scans were carried out in a hexagonal grid using 1.5 to 5 μm step sizes over areas approximately 200×200 to 500×500 μm^2 in dimensions. OIM data

included the Cartesian coordinate location of each orientation corrected for the 70° tilt of the sample, the Euler angles representing the orientation, a measure of the image quality of the backscattered diffraction pattern, and a measure of the confidence in indexing of the backscatter diffraction pattern (confidence index). Plots were produced of confidence index as a function of position and overlaid with boundaries in the range of 2°–15° (low-angle) and 15°–180° (high–angle). Boundaries were color coded to aid identification as follows: Σ1-blue, Σ3-red, Σ9-yellow, Σ27-green, other Σ-brown, random-black. This is also the scheme followed in Figures 2 and 3 later in the paper. The Brandon criterion [25] was applied to identify those boundaries, which were special in nature using tables produced by Adams *et al.* [27]. The average angular deviation from exact misorientation was calculated for each special orientation, and the results been shown earlier in Refs. 23 and 24. Data was acquired from 2-5 areas for each heat treatment allowing for error bars corresponding to 1-σ uncertainty to be placed on the GBCD results.

The OIM data was further analyzed using software developed at Lawrence Livermore National Laboratory in the IDL 5.0 (Research Systems, Inc.) interactive data language program. The first step in data analysis was to treat data points with a low confidence index (<0.1). Confidence index is a measure of the certainty of the pattern indexing. Work at TSL, Inc. has shown that the uncertainty in indexing of a backscatter electron diffraction pattern is nearly constant for confidence indices greater than 0.1, whereas the uncertainty increases precipitously for lower confidence indices [26]. An algorithm was developed to associate the orientation of a low confidence index point with that of the majority of its neighbors with common orientation. For example, it is likely that a low confidence index point will have several neighbors of common orientation. The misorientations of the six neighbors of the low confidence index point are assessed and the largest number of common-orientation, contiguous neighbors is determined. The orientation of the low confidence index point and its confidence index are re-assigned from the maximum confidence index point in the list of largest number of common-orientation contiguous neighbors.

The OIM data was then corrected for points with acceptable confidence index that were likely mis-indexed, such as a single point in the center of a large grain whose orientation differs from its neighbors. First, each data point was surveyed to determine the number of neighbors with differing orientation from the data point (misorientation > 15°). If that number was five or six, the point was considered for correction of the orientation. The neighbors were then surveyed to determine the largest number of contiguous neighbors with common orientation. If that number was five or six, then the point in question was assigned the average orientation of those five or six neighbors.

OIM images using the TSL, Inc. data acquisition software and hardware are acquired on a hexagonal grid. Thus, each orientation point can be represented as a hexagonal Voronoi cell. Neighboring hexagons meet at triple nodes. This geometry is ideal for identifying triple junctions in the microstructure: the intersection of three hexagons. Because of the geometry, quadruple nodes cannot occur. Plots were produced identifying the location of low-confidence-index orientation points as a function of position and overlaid with boundaries. The Brandon criterion [25] was applied to identify those boundaries that were special in nature using tables produced by Adams *et al.* [27]. Boundaries with Σ≤49 were considered to be special while boundaries with Σ>49 were considered random. The data were then surveyed to identify the location of triple junctions in the data set. A triple junction was identified as a triple node in the hexagonal array where three boundaries intersect. The triple points were characterized after Fortier *et al.* [28] and parsed among four groups: three special boundaries (S-S-S), two special boundaries and one random boundary (S-S-R), one special and two random boundaries (S-R-R), and three random boundaries (R-R-R).

RESULTS AND DISCUSSION

The grain boundary character distributions obtained from OIM images are presented in Figures 1, 4 and 5. Subsequent analysis of the OIM data also yielded the triple junction distributions and these are also plotted in Figures 1, 4, 5, and 6.

Strain Annealing

The initial grain size for the strain-annealed ofe-Cu was ~10 μm and exhibited a special fraction of approximately 0.66, *i.e.*, the ratio of the total number of boundaries in the range

$1 \leq \Sigma \leq 49$ to the total number of boundaries sampled. This is due to the multiple deformation and recrystallization steps involved in producing the starting plate, which improved the GBCD compared with the starting material. Figure 1 summarizes the GBCD results for the four strain-annealing treatments as well as the starting as-recrystallized material. The SA-1 treatment led to an abnormally large fraction, almost 50%, of $\Sigma 1$ boundaries and hence to permit better comparison with the other samples the fraction of $\Sigma 1$ boundaries has been omitted from consideration. Thus, the fraction of other special boundaries is artificially inflated in the plot. It is seen that there are very few $\Sigma 9$ and $\Sigma 27$ boundaries present after the anneal, and the relative proportion of other special boundaries goes down as well. This annealing treatment was accompanied by a significant and undesirable increase in grain size. Also, SA-1 exhibited a larger statistical spread in special fraction and deviation angle from exact Σ misorientation than SA-2, SA-3, and SA-4 [23,24]. The 7% compression resulted in an increase in the average deviation from ideal misorientation for the $\Sigma 3$, $\Sigma 9$, and $\Sigma 27$ boundaries and the subsequent annealing steps resulted in only an insignificant change in the deviation [23,24].

The SA-2, SA-3, and SA-4 strain-annealing treatments exhibited significantly different behavior than SA-1. In these cases, after the final anneal, the $\Sigma 3$ fraction increases slightly, with proportionate increases in the $\Sigma 3^n$ and total special boundary fractions. In contrast to SA-1, the deviation from exact misorientation is observed to decrease significantly during the final anneal [23,24]. The special fractions for these latter experiments approached 75%.

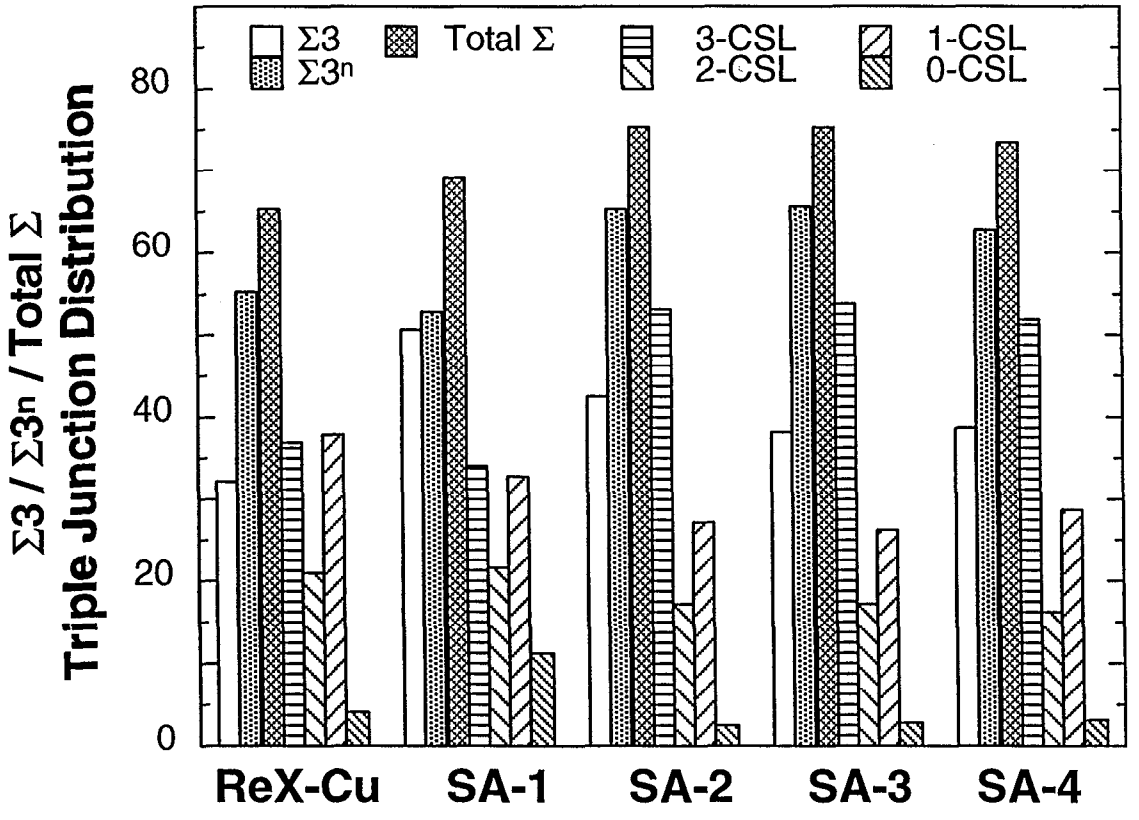

Figure 1. Grain boundary character and triple junction distributions for strain-annealed ofe-Cu as a function of different processing sequence as given in Table II.

Figure 1 also plots the number of 3-CSL, 2-CSL, 1-CSL, and 0-CSL triple junctions. Favorable trends were observed in the SA-2, SA-3, and SA-4 strain-annealing treatments. The number of 3-CSL boundaries increases significantly from the as-recrystallized and SA-1 treatments. This rise in 3 CSL triple junctions is accompanied by a corresponding decrease in the less desirable 1-CSL and 0-CSL triple junctions.

Two fundamentally different approaches to optimization of the GBCD in ofe-Cu and Inconel 600 are described in this section. The strain-annealing (SA) treatment, which does not

induce complete recrystallization due to low deformation strain, has been found in this study to be capable of increasing the overall fraction of special boundaries and reducing the average deviation from the exact Σ misorientation [23,24]. This result is similar to the work of Randle and Brown [14], Lim and Raj [21] and Thomson and Randle [22]. The reduction of the average deviation of $\Sigma 3$ boundaries, or "fine–tuning" as suggested by Thomson and Randle [22], occurs as a result of a lowering of energy through reduction in the boundary curvature of the vicinal boundaries. As expected, the frequency of $\Sigma 3$ boundaries changes only slightly, with the biggest increase of about 10% seen for the SA-2 treatment. The special fraction increases only modestly as well. Similar trends were observed [23,24] when the special fractions were considered in terms of the total length of boundaries rather than by their frequency. However, the fraction of $\Sigma 3$ boundaries was as high as 50–60% compared with 35–40% when the measurement is by frequency of occurrence. This is a clear indication of a lower energy state being achieved by an increase in the length of low-energy $\Sigma 3$ boundaries at the expense of relatively higher energy boundaries rather than an increase in their numbers. It is interesting to note in this context that the fraction of $\Sigma 9$ and $\Sigma 27$ boundaries decreases considerably when measured by length. This concurs with the suggestion [22] that the fine-tuning associated with $\Sigma 9$ and $\Sigma 27$ boundaries occurs as a necessity of geometrical considerations during the recombination of two $\Sigma 3^n$ boundaries, such as the $\Sigma 3 + \Sigma 3 = \Sigma 9$ reaction, and not because of a reduction in total energy of the grain boundary network. Such reactions have been shown in the OIM image of Figure 2, including cases where a $\Sigma 27$ boundary segment has been created by the reaction of a $\Sigma 3$ and $\Sigma 9$ boundary. Also shown are the cases where annealing twinning has favorably altered the character of a randomly oriented boundary to that of special character.

The fraction of $\Sigma 1$ boundaries remained about the same as in the as-recrystallized starting material with an increase seen only during the SA-1 treatment, which also served to enhance the special fraction in SA-1 above the others. This increase in $\Sigma 1$ boundaries, mostly in the range of 2–5°, in the SA-1 treatment could be due to enhanced grain boundary migration and hence increased grain growth at the higher temperatures ($0.45T_m$ for 8 hours followed by $0.6T_m$ for 14 hours) used in this particular experiment. In the other cases, since the temperatures are kept below $0.5T_m$ grain boundary migration is less probable and the frequency of $\Sigma 1$ boundaries in these samples is consistent with that observed in the starting fully recrystallized material. It is also conceivable that the increase in $\Sigma 1$ boundaries after the SA-1 treatment is due to localization of strain through lattice rotations within individual grains [29,30], which is far more common during deformation processes.

In contrast to the results of Thompson and Randle [22] strain annealing under the conditions examined here led to significant grain growth as shown in Table II. Grain growth was most pronounced in SA-1, which had the highest heat treatment temperatures. However, grain growth also occurred to a lesser degree in the other three strain-annealed samples. It is not surprising that grain growth is observed along with a reduction in the deviation from the ideal misorientation since both the processes arise from a common phenomena, *i.e.*, reduction in grain boundary curvature or the energy of the interfaces.

Other mechanisms that could be active in promoting the increase in the special boundary fraction are grain rotation and local lattice rotations. Local lattice rotations do play a large role during deformation or in accommodation of constraints near interfaces or grain boundaries, as shown in Figure 3. A comparison between the GBCD of the solution treated material (Figure 3a) and deformed about 15% in compression (Figure 3b) suggests that considerable local rotation within the grains is encountered during deformation, as evidenced by the increased frequency of $\Sigma 1$ boundaries. Moreover, local changes in the misorientations of the existing high angle boundaries are observed at locations where $\Sigma 1$ boundaries have intersected these boundaries. This appears to modify the character of the boundary locally; in some cases converting randomly oriented boundaries into ones with special CSL character. Similarly, it is observed that $\Sigma 3$ boundaries are locally modified into random boundaries by the development of local misorientations (<15°) near them. These findings are similar to the recent observations made by Sun *et al.* [30] on Al bicrystals, though local modifications in the character of the boundaries were not observed at lower levels of deformation (~10%). Of course, even higher deformations (>40-50%) will lead to the formation of high energy, high angle boundaries within individual grains in the microstructure [31], but these high strain levels are not considered relevant to the study of GBCD optimization.

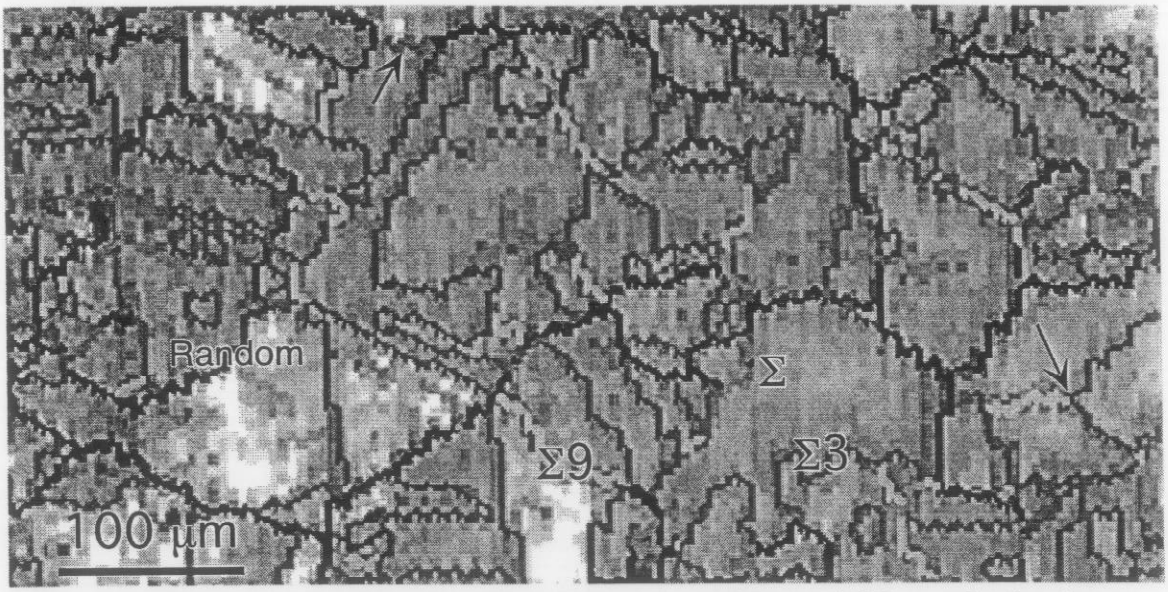

Figure 2. OIM image of a thermo-mechanically processed Inconel 600 sample showing reactions between twin variants, and also the modification of segments of random boundaries to those of special character on intersections with annealing twins. Boundaries are marked as follows: Σ1-blue, Σ3-red, Σ9-yellow, Σ27-green, other Σ-brown, and random-black.

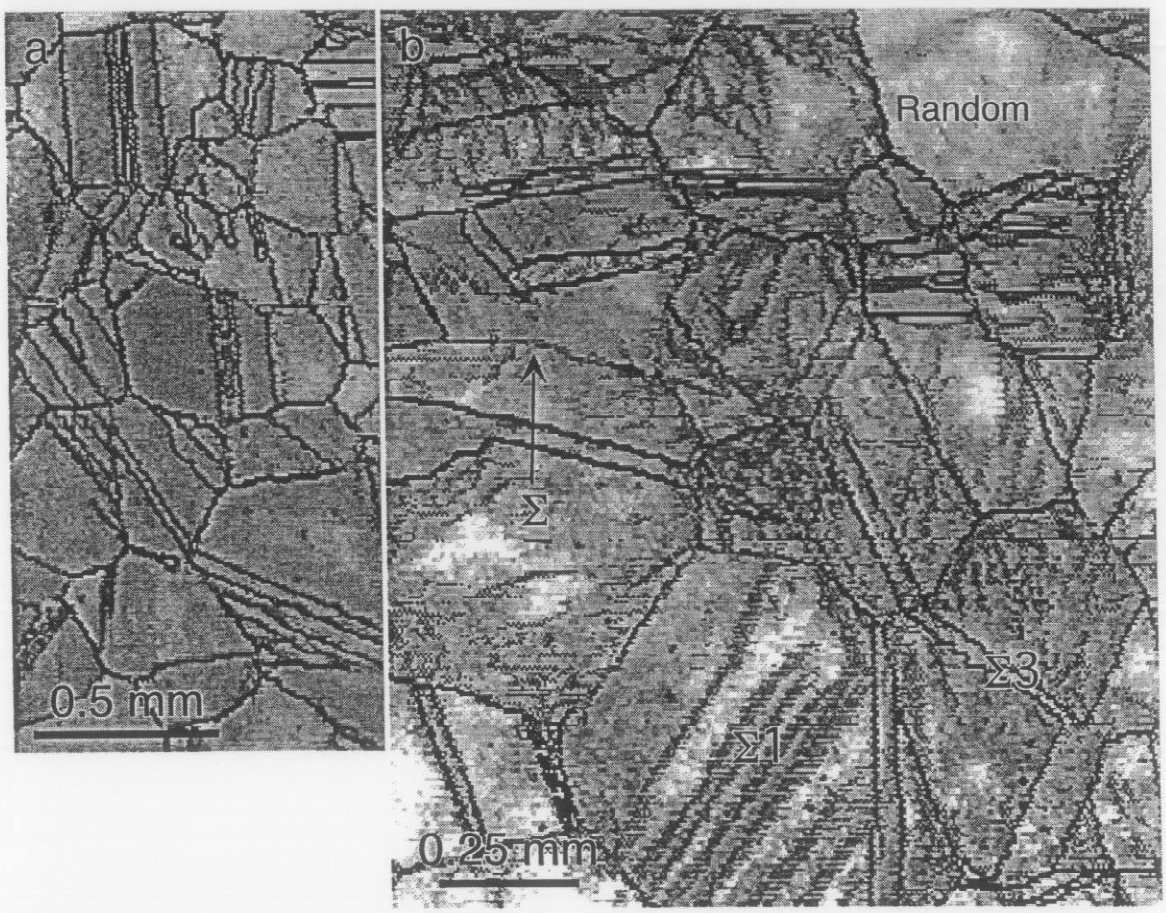

Figure 3. OIM image showing the GBCD in Inconel 600: a) solution treated sample with low fraction of Σ1 boundaries (blue), and b) 15% compressed sample with high density of low angle (2°–5°) boundaries as a consequence of lattice rotation during deformation. Boundaries are color-coded as in Figure 2 above.

An OIM examination of the SA-2 processed material indicated that the very high special fraction (by length but not by frequency of boundaries) reflects a second phenomena in addition to the connectivity of the special boundaries in the microstructure. Numerous "island twins" are observed which tend to skew the $\Sigma 3$ statistics to higher levels without enhancing the two-dimensional grain boundary network structure. These "island twins" do not contribute to the optimization of the GBCD in terms of approaching the so-called twin-limited microstructure [14,15] since they do not interrupt the connectivity of random boundaries at triple junctions. The origin of these "island twins" is a matter of some speculation [32], with one of the suggestions being that they are formed by inter-penetration of annealing twins on intersecting planes. However, it is not inconceivable that they are cross-sections of twins that appear as isolated entities on the planar surface of the microstructure sampled in the SEM.

Strain Recrystallization

The starting material for the strain-recrystallization study was ofe-Cu in the semi-hard condition with a grain size on the order of ~125 μm, but with a few individual grains larger than 500 μm. Therefore, a very high fraction of $\Sigma 1$ boundaries was expected in the deformed state. The very low fraction of $\Sigma 3$ boundaries, as shown in Figure 4 is rather surprising in light of the low stacking fault energy (~60-70 mJ/m^2) in copper. After the first strain-recrystallization treatment, only the SR-1-400 material (strain-recrystallization at 400°C for 10 minutes, 1 deformation-anneal treatment) was examined using OIM. This heat treatment provided a large increase in the $\Sigma 3$ boundaries with a steep drop in the $\Sigma 1$ boundaries. After the second and third compression-heat treatment (SR-N-xxx, where N is the heat treatment number) OIM was performed on all specimens. Figures 4(a,b) demonstrate how the special fraction increases with successive processing using the SR-N-350 and SR-N-400 strain-recrystallization combinations, respectively. These optimization treatments successfully increase the number of $\Sigma 3$ boundaries, the number of $\Sigma 3^n$ boundaries, as well as the total special fraction to approximately 65% by percentage. In contrast, the percentage calculated by length of special boundaries is approximately 75% as previously reported [23,24]. Also plotted in Figure 4 are the triple junction distributions.

Thermomechanical processing of the Inconel 600 alloy by repeated strain-recrystallization resulted in significant changes in the special fractions and triple junction distributions shown in Figure 5. The total special fraction, fraction of $\Sigma 3^n$ boundaries, and percentage of 3-CSL triple junctions are observed to increase dramatically with processing step. The 1-CSL and 0-CSL boundaries exhibit a corresponding decrease.

The strain recrystallization sequences studied for ofe-Cu and Inconel 600 appear to be a more effective method of increasing the special fraction (with little island twinning), while reducing the grain size. Since the starting material (ofe-Cu) was in the semi-hard condition, an additional 30% compression deformation induced full recrystallization at 400°C, with a gradual increase in the fraction of $\Sigma 3$ boundaries and a dramatic rise in the fraction of $\Sigma 9$ and $\Sigma 27$ boundaries. This was accompanied by a considerable lowering of the numbers of low-angle boundaries in the microstructure. At the same time, the grain size decreased to below 50 μm. Subsequent deformation-recrystallization treatments at this temperature also induced recrystallization but with only a minor reduction in grain size. The results from samples deformed to the same level but recrystallized at 350°C and 375°C were similar to 400°C samples, with a marginally higher special fraction at the lower temperatures due to a slight increase of about 3-4% in the $\Sigma 3$ fraction. The ratio of $\Sigma 9$ and $\Sigma 27$ boundaries to twin boundaries goes up with increasing number of strain recrystallization cycles. This is indicative of an increasing number of multiple twinning or twin intersection events, of the type shown in Figure 2, as these $\Sigma 3^n$ boundaries arise from the geometrical necessity of connecting $\Sigma 3$ boundaries in the grain boundary network.

A comparison between the ofe-Cu strain recrystallization and SA-4 treatments shows that a higher percentage increase in the special fraction can be achieved by high-strain, short-time treatments than by strain annealing cycles of low strains and long thermal treatments. Preferential nucleation of lower energy, low CSL boundaries during recrystallization is only possible through storage of cold work sufficient to induce changes in the microstructure of the kind seen in Figure 3. The slightly higher numbers in the SA treatments only come about due to the better distribution in the fully recrystallized starting material. The striking point is that the frequency of $\Sigma 3$ boundaries in both cases levels off at approximately 35-40% of the total

number of boundaries, with the ratio of Σ3 boundaries to Σ9 and Σ27 boundaries also peaking at a value of 3:2.

Not surprisingly, the analysis of the Inconel 600 samples revealed similar trends to those seen for ofe-Cu even though the recrystallization temperature normalized with respect to the melting temperature (~0.8Tm) was much higher in this case. The most notable difference is a slight drop in the fraction of higher order $\Sigma 3^n$ boundaries, even though the fraction of annealing twin boundaries is roughly the same. The reason for this apparent decrease could not be ascertained and could very well be statistical in nature.

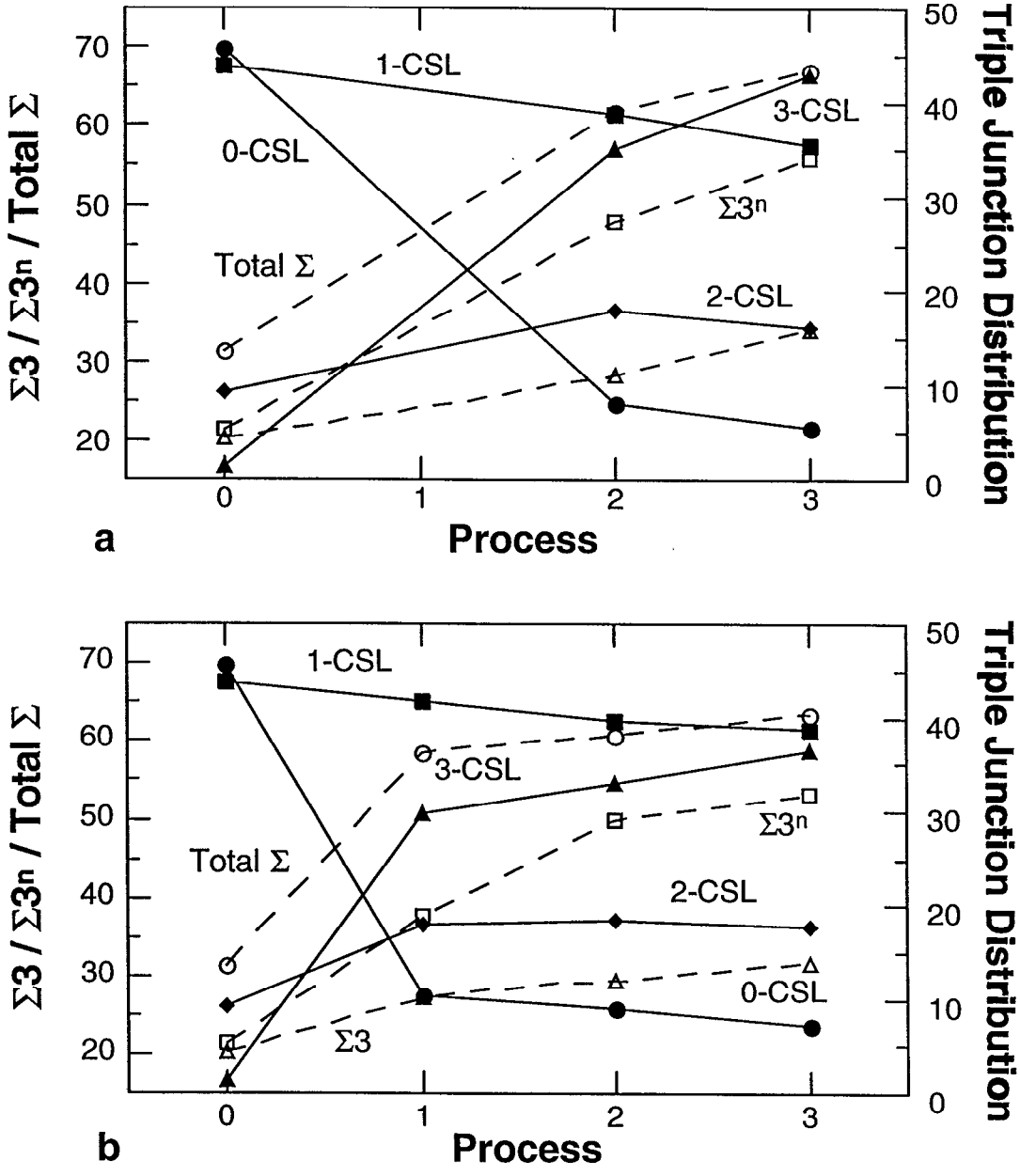

Figure 4. Grain boundary character and triple junction distribution for strain-recrystallized ofe-Cu as a function of process cycle number at, a) 350°C and b) 400°C. Note that the open data points and dashed lines represent the left-hand axis and the closed data points and solid lines represent the right-hand axis.

The results described in this study are in good agreement with the data reported in the literature on GBCD optimization in Ni-base alloys, Cu and austenitic stainless steels [33,34].

As an example, a comparison of a study on Inconel 600 by Lin *et al.* [33] shows that the special fraction after the GBE™ (registered trademark of Ontario Hydro Technologies, Toronto, Canada) treatment reaches an average value of 67%, which compares favorably with the results obtained in this study. The Σ3 fraction, however, is lower than that reported by Lin *et al.*, though the other $\Sigma 3^n$ boundaries are much higher in comparison. It should be noted here that quite often it is not clearly stated whether the experimental approach reports the fraction of boundary length or the frequency of occurrence of a particular grain boundary type. As has been stated in the literature [35], and also mentioned earlier, consideration in terms of the boundary length results in an increase in the Σ3 and special fraction distributions obtained in this study and brings the GBCD in close agreement with the results of Lin *et al.* [33].

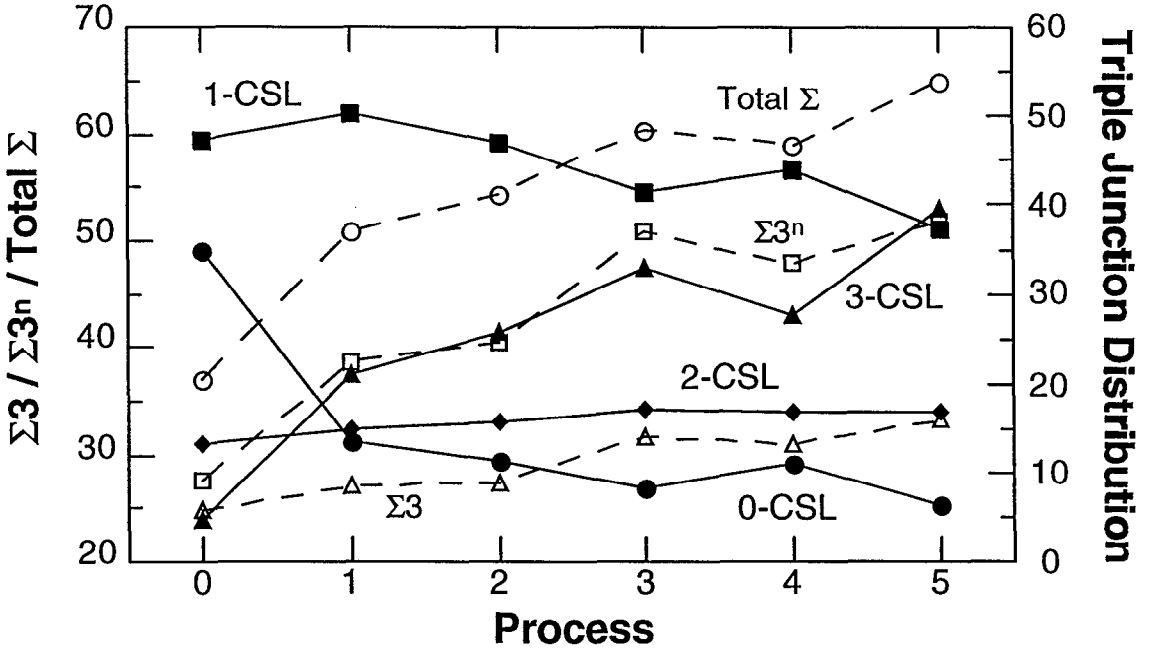

Figure 5. Grain boundary character and triple junction distribution for strain-recrystallized Inconel 600 as a function of process cycle number. Note that the open data points and dashed lines represent the left-hand axis and the closed data points and solid lines represent the right-hand axis.

Regardless of the approach, it appears that the optimum processing conditions have not been attained during the strain recrystallization treatments in this study. This is evidenced by the fact that the ratio of Σ3 to other $\Sigma 3^n$ boundaries levels off very early on in the thermomechanical cycle and never approaches the distribution specified by an ideal twin-limited microstructure [14,15]. In the twin limit, the fraction of Σ3 boundaries approaches the limit of $^2/_3$, with the remainder of boundaries consisting entirely of Σ9 and Σ27 types and possibly a few Σ1 boundaries. Gertsman and Szpunar [31] have suggested that at a minimum the sum of Σ1 and Σ9 boundary fractions should be equal to the fraction of Σ3 boundaries less $^1/_3$, provided the frequency of Σ3 boundaries exceeds $^1/_3$. This evaluation is based on the assumption that in an idealized microstructure with a spatial distribution consisting only of triple junctions the maximum possible fraction of Σ3 boundaries until they impinge on each other is $^1/_3$. As this number increases beyond $^1/_3$ twin-twin interactions increasingly become common leading to the formation of Σ1 or $\Sigma 3^n$ boundaries. Interestingly, the distributions encountered in this study have a close resemblance to the computer simulation results of Gertsman and Tangri [36] on multiple-twinned structures in a range of about 4-5 twins per initial grain.

Triple Junction Distribution

The idea of grain boundary design has primarily meant the engineering of polycrystalline materials properties through alteration of the grain boundary character distribution. However, modifications in the GBCD are a necessary, but not sufficient,

condition to impact properties such as fracture characteristics, which are primarily dependent on the spatial distribution and interconnectivity of the boundaries prone to crack propagation. In this light, in quantifying the effect of twinning on the CSL distribution it is also necessary to evaluate how even a single twin can affect the crystallography of the neighboring interfaces in a reference tetrakaidekahedral crystal [37]. Clearly, the polycrystalline ensemble cannot be treated as a collection of isolated bicrystals or tricrystals since the twin boundaries exert an influence on the grain boundary network beyond their nearest neighbors. In an ideal case, it has been suggested [14,15], that the space filling operation can be carried out in the manner of the twin limited microstructure assuming that only triple points or nodes exist in the polycrystalline ensemble. In a modification to this, Miyazawa *et al.* [16] have suggested that a three-dimensional polycrystal can be entirely composed of grains that adopt the shape of truncated octahedron with only $\Sigma 3$ and $\Sigma 9$ boundaries or $\Sigma 3$, $\Sigma 5$ and $\Sigma 15$ boundaries.

The resultant microstructure is considered to be important in the improvement of the grain boundary character distribution and also the development of a triple junction distribution that breaks the connectivity of the random boundary network, or in the ideal case eliminates it altogether. To this end, the triple junction (or line) distribution was evaluated for the variously processed materials in this study. The exact nature of the triple point (or line) in the manner of the I-line/U-line or coincident axial direction (CAD) descriptions was not attempted, but rather the distribution of the three boundaries at the junction, as in Ref. 29, was evaluated. These results have been plotted in Figures 1, 4 and 5, and also of triple junction distributions as a function of special fraction in Figure 6 for all the materials considered in this study.

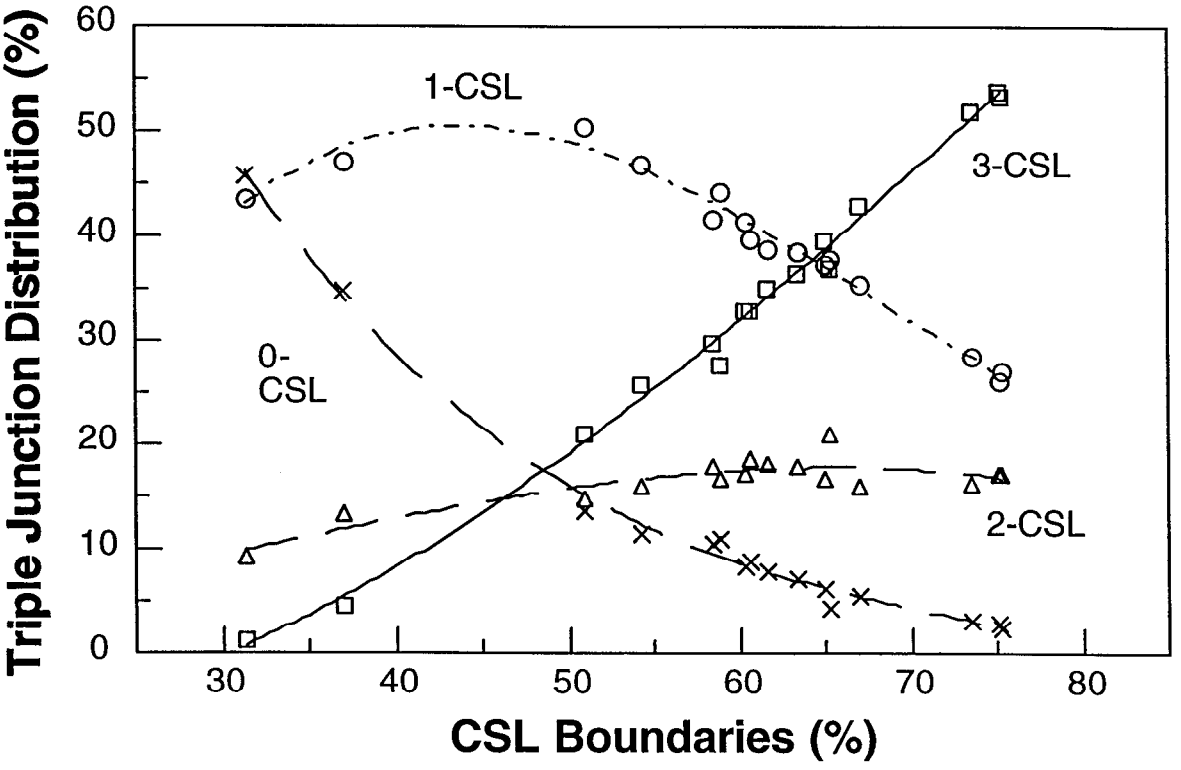

Figure 6. Triple junction distributions by junction type as a function of the proportion of special boundaries in strain-annealed and strain-recrystallized ofe-Cu and Inconel 600.

Figure 1 shows the triple junction distribution in strain-annealed ofe-Cu for the various heat treatment schedules. In all three cases, SA-2, SA-3 and SA-4, it is clear that an increase in the $\Sigma 3$ fraction promotes the formation of triple junctions comprising of 3 CSL boundaries. But the increase is not proportionate, which indicates that the multiple twinning events also promote the formation of other $\Sigma 3^n$ variants, like $\Sigma 9$ and $\Sigma 27$, in the microstructure. It is also seen that the percentage of 2-CSL junctions goes down significantly along with the proportion of 1-CSL junctions. The initial microstructure, being fully recrystallized, did not contain many junctions

that were comprised of only random boundaries and hence this fraction did not show any significant drop on strain annealing. The results from SA-1 were at variance from the other three cases, perhaps reflecting the increase in $\Sigma 1$ boundaries within individual grains. Numerous $\Sigma 1$-$\Sigma 1$-$\Sigma 1$ junctions could be observed in the microstructure, thus artificially boosting the fraction of 3-CSL junctions without providing an improvement in the random boundary network. When the $\Sigma 1$ boundaries are not included in the analysis the fraction of 3-CSL junctions goes down quite a bit.

The triple junction distributions in the strain-recrystallized samples (Figures 4 and 5) were a bit different from the previous case. In all cases a dramatic drop was observed in the 0-CSL fraction from the value for the starting material, eventually leveling off just below 10% of the total number of the triple junctions. A slight decrease in the fraction of 1-CSL junctions was also commonly seen with an increase in the special fraction in the microstructure. Surprisingly, the 2-CSL distribution stayed level throughout the processing sequence at about 20-25%, though the 3-CSL fraction showed a very significant increase with a maximum value of about 44%. This indicates an increasingly higher level of twin-twin interactions to provoke the formation of $\Sigma 3^n$ variants. On evaluating the effect of temperature of processing on the ofe-Cu samples (Figure 4), it was noted that the fraction of 3-CSL junctions was higher by 7% in samples processed at the lower temperature, though the distributions of 1-CSL and 2-CSL junctions were almost identical. This perhaps is a consequence of the marginally higher special fraction in the lower temperature sample.

It was mentioned in the introductory section that very few studies [28,35] have been reported of comparison between GBCD with triple junction distributions for experimentally determined data sets. Moreover, in the simulations of the triple junction distribution by Fortier *et al.* [28] the spatial connectivity of these junctions has not been included. Instead, independent sets of three orientations were used for the determination of triple junction classifications. Nevertheless, on comparing the results obtained in this study with computer simulated observations or probability calculations of Fortier *et al.*, it is clear that that there is good agreement with respect to the trend and absolute distribution of 3-CSL junctions with proportion of special boundaries (Figure 6). Interestingly, the 0-CSL distribution also is in good agreement with the simulated results. This finding is not all that surprising since these two distributions are only weakly dependent on spatial correlations of their constituent boundaries beyond their nearest neighbors, unlike the other two distributions.

The results from this study show significant departure with the simulations of Fortier *et al.* [28] when the 2-CSL and 1-CSL distributions are considered. The computer simulations show that the proportion of 2-CSL junctions should increase as the special fraction goes up, but clearly that is not exhibited experimentally. Moreover, the absolute values obtained here are much lower in comparison. Significantly, the experimentally measured distributions of 1-CSL junctions are higher than the predicted values from simulations or analytical calculations. These observations emphasize the point that the functions are strongly correlated with the overall distribution of grain boundaries in a polycrystalline ensemble.

Computer simulations [38], not described in this paper for the sake of brevity, were also conducted in the manner of Fortier *et al.* [29] to emulate the distributions obtained by them. However, when spatial correlations between triple junctions are strictly enforced, *i.e.*, the CSL designations of grain boundaries are applied based on the combination rules designed by Bollmann [39], then the distributions are in good agreement with the experimental results shown here. Moreover, it was evident that enforcing the combination rule alone at an isolated triple junction was insufficient to explain the triple junction distribution obtained experimentally, though the simulated results more closely resemble this distribution than what was reported by Fortier *et al.* [28].

It was mentioned earlier in the paper that it does not appear as if the GBCD in these materials has been optimized on the basis of the ideal twin-limited microstructure. Nevertheless, the triple junction distributions show that almost 40% and 20% of the junctions are comprised of 3 and 2 special boundaries, respectively. Thus there is a strong argument to believe that the connectivity of random boundaries is getting reduced to shorter path lengths. The problem then remains of finding an appropriate function that describes when the assembly of random boundaries reaches a critical value. Wells *et al.* [40], on the basis of a bond percolation formulation suggested that the minimum fraction of random boundaries that will

lead to the formation of a continuous linear chain was 0.23. However, when a planar section is considered, based on an approximation of the two-dimensional microstructure to a honeycomb network, then this boundary fraction has to be at least 0.65. On this basis, it is apparent that the connectivity of the random grain boundary networks has been broken in the materials studied here. However, the caveat lies in the purely probabilistic approach and the fact that it does not address the possible correlations that exist in a grain boundary network. Moreover, the path length that is assumed in the analysis may be an overestimation of the critical length in the materials phenomenon in consideration.

CONCLUSIONS

It has been demonstrated that the fraction of special boundaries in ofe-Cu and Inconel 600 can be increased through thermomechanical processing like strain-annealing or strain-recrystallization. Using commercially practical processing methods, it is possible to increase special fractions to over 70%, while the grain size decreases and no significant texture develops or is randomized. The new microstructure is composed of a network of random boundaries interrupted by special boundaries through the process of multiple twinning and formation of $\Sigma 3^n$ variants. It is concluded that annealing twinning alone cannot account for the optimization of the microstructure unless the twin-related variants appear in the microstructure and increase the fraction of triple junctions that are composed of at least two special boundaries.

ACKNOWLEDGEMENTS

The assistance of E. Sedillo, L. Nguyen, and the metallography of R. Kershaw are gratefully acknowledged. This work was performed under the auspices of the U.S. Department of Energy and Lawrence Livermore National Laboratory under contract# W-7405-Eng-48.

REFERENCES

1. P. Lin, G. Palumbo, U. Erb, and K. T. Aust, *Scripta Metall. Mater.*, **33**, p. 1387 (1995).
2. G. Palumbo and K. T. Aust, *Can. Metall. Qtrly.*, **34**, p. 165 (1995).
3. G. Palumbo, P. J. King, K. T. Aust, U. Erb, and P. C. Lichtenberger, *Scripta Metall. Mater.*, **25**, p. 1775 (1991).
4. J. Don and S. Majumdar, *Acta Metall.*, **34**, p. 961 (1986).
5. E. M. Lehockey, G. Palumbo, A. Brennenstuhl, and P. Lin, *Mater. Res. Soc. Symp. Proc.*, **458**, p. 243 (1997).
6. L. C. Lim and T. Watanabe, *Acta Metall.*, **38**, p. 2507 (1990).
7. M. Kumar, A. J. Schwartz, and W. E. King, unpublished research (1998).
8. *JOM*, February 1998, pp. 39-59.
9. T. Watanabe, *Res. Mech.*, **11**, p. 47 (1984).
10. H. Grimmer, W. Bollmann, and D. H. Warrington, *Acta Cryst.*, **A30**, p. 197 (1974); D. H. Warrington and M. Boon, *Acta Metall.*, **23**, p. 599 (1975).
11. V. Randle, *Acta Mater.*, **46**, p. 1459 (1997).
12. G. Gottstein, *Acta Metall.*, 32, p. 1117 (1984).
13. A. Berger, P. J. Wilbrandt, F. Ernst, U. Klement, and P. Haasen, *Prog. Mater. Sci.*, **32**, p. 1 (1988).
14. V. Randle and A. Brown, *Philos. Mag.*, **A59**, p. 1075(1989).
15. G. Palumbo, K. T. Aust, U. Erb, P. J. King, A. M. Brennenstuhl, and P. C. Lichtenberger, *Phys. Stat. Sol.* (a), **131**, p. 425 (1992).
16. K. Miyazawa, Y. Iwasaki, K. Ito, and Y. Ishida, *Acta Cryst.*, **A52**, p. 787 (1996)
17. G. Palumbo and K. T. Aust, *Acta Metall. Mater.*, **38**, p. 2343 (1990).
18. R. D. Doherty, I. Samajdar, and K. Kunze, *Scripta Metall. Mater.*, **27**, p. 1459 (1992).
19. B. L. Adams, *Mater. Sci. Engg.*, **A166**, p. 59 (1993).
20. B. L. Adams, S. I. Wright, and K. Kunze, *Metall. Trans.*, **A24**, p. 819 (1993).
21. L. C. Lim and R. Raj, *Acta Metall.*, **32**, p. 117 (1984).
22. C. B. Thomson and V. Randle, *Acta Mater.*, **45**, p. 4909 (1997).
23. W. E. King and A. J. Schwartz, *Mater. Res. Soc. Symp. Proc.*, **458**, p. 53 (1997).
24. W. E. King and A. J. Schwartz, *Scripta Mater.*, **38**, p. 449 (1998).
25. D. G. Brandon, *Acta Metall.*, **14**, p. 1479 (1966).
26. TSL, Inc. Orientation Imaging Microscopy Software Version 2.5 User Manual (Draper, UT: TSL, Inc. (1997).

27. B. L. Adams, J. Zhao, and H. Grimmer, *Acta Cryst,*. **A46**, p. 620 (1990).
28. P. Fortier, W. A. Miller, and K. T. Aust, *Acta Mater.*, **45**, p. 3459 (1997).
29. V. Randle, N. Hansen, and D. Juul Jensen, *Philos. Mag.*, **A73**, p. 265 (1996).
30. S. Sun, B. L. Adams, and W. E. King, in preparation (1998).
31. B. Bay, N. Hansen, D. A. Hughes, and D. Kuhlmann-Wilsdorf, *Acta Metall. Mater.*, **40**, p. 205 (1992).
32. J. Bystrzycki, W. Przetakiewicz, and K. J. Kurzydlowski, *Acta Metall. Mater.*, **41**, p. 2639 (1993).
33. P. Lin, G. Palumbo, and K. T. Aust, *Scripta Mater.*, **36**, p. 1145 (1997).
34. V. Y. Gertsman and J. A. Szpunar, *Scripta Mater.*, **38**, p. 1399 (1998).
35. V. Y. Gertsman, K. Tangri, and R. Z. Valiev, *Acta Metall. Mater.*, **42**, p. 1785 (1994).
36. V. Y. Gertsman and K. Tangri, *Acta Metall. Mater.*, **43**, p. 2317 (1995).
37. D. McLean, *Grain Boundaries in Metals*, Clarendon Press, Oxford, England (1957).
38. W. E. King, M. Kumar, and A. J. Schwartz, unpublished research (1998).
39. W. Bollmann, *Crystal Lattices, Interfaces, Matrices*, Geneva (1982).
40. D. B. Wells, J. Stewart, A. W. Herbert, P. M. Scott, and D. E. Williams, *Corrosion*, **45**, p. 649 (1989).